Supplementary Information for:

Targeting 17q23 amplicon to overcome the resistance to anti-HER2 therapy in HER2+ breast cancer

Liu *et al.*

Includes: Supplementary Figures 1-9

Supplementary Table 1

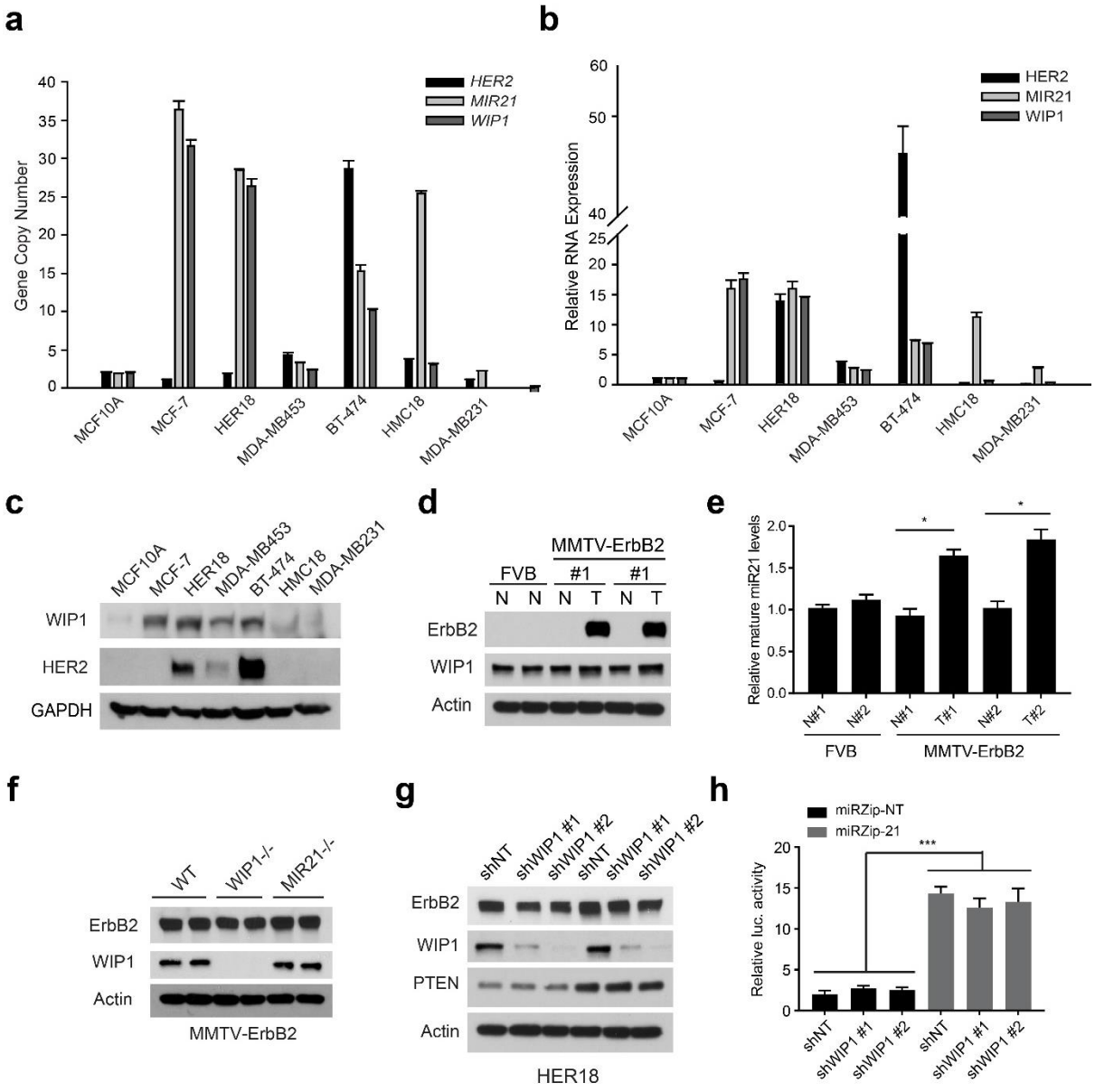

Supplementary Figure 1. Co-amplification of *WIP1* and *MIR21* in the 17q23 amplicon of HER2+ breast cancer cell lines. (**a, b**) Copy numbers (**a**) and relative RNA expression levels (**b**) of *HER2, WIP1* and *MIR21* in a panel of breast cancer cell lines. The non-tumorigenic epithelial cell line MCF10A was used as a control. (**c**) Protein expression levels of HER2 and WIP1 in a panel of breast cancer cell lines as determined by Western blot. (**d, e**) Expression levels of WIP1 (**d**) and mature miR-21 (**e**) in the normal mammary tissue (N) or mammary tumor (T) of *MMTV-ErbB2* mice. Normal mammary tissue collected from control FVB mice was analyzed as a control. (**f**) Protein expression levels of ErbB2 and WIP1 in the mammary tumors from *MMTV-ErbB2, WIP1−/−;MMTV-ErbB2* and *MIR21-/-;MMTV-ErbB2* mice. (**g, h**) Protein

expression levels of HER2 in HER18 cells with stable knockdown of WIP1, miR-21 or both (**g**). Knockdown efficiency of miR-21 in HER18 cells was measured by luciferase reporter assay (**h**). The luciferase activity of the reporter gene with miR-21-targeting 3'-UTR is negatively correlated with the level of miR-21. * $p<0.05$; *** $p<0.001$; unpaired 2-tailed *t*-test (**e, h**). Data are presented as mean ± SD and are representative of 3 independent experiments.

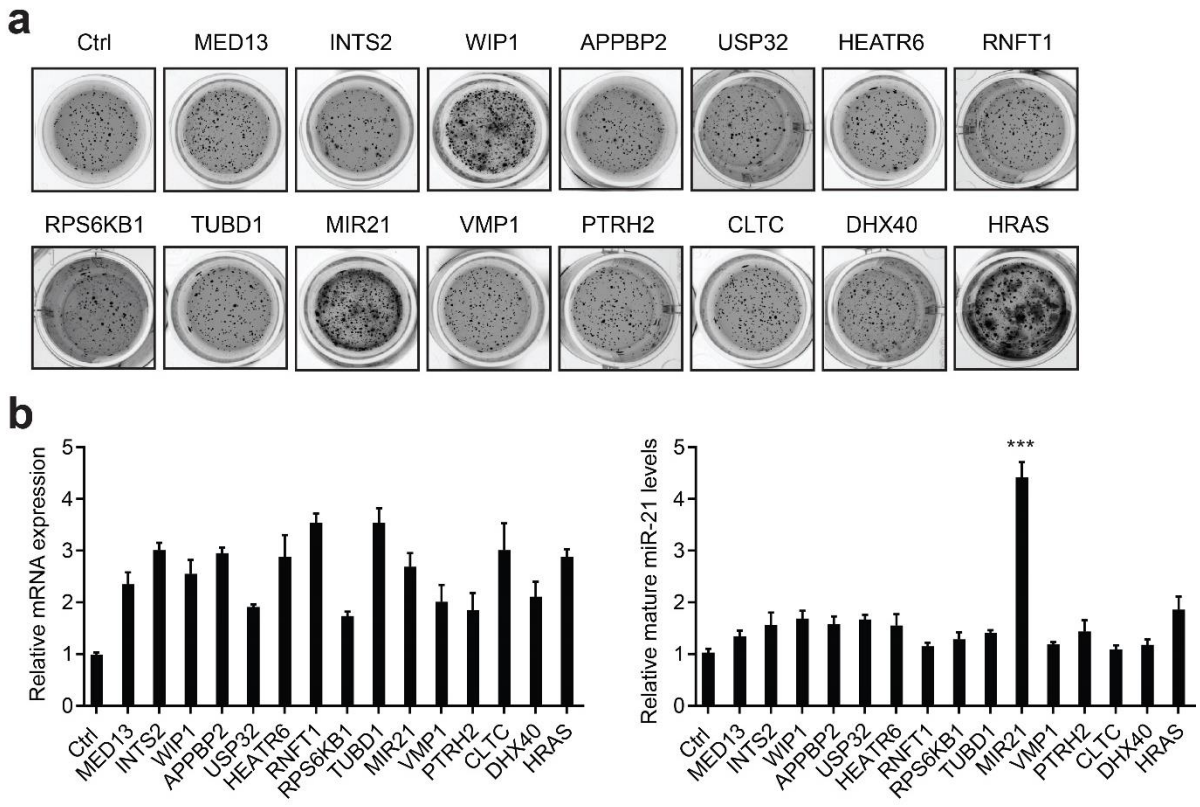

Supplementary Figure 2. Overexpression of *WIP1* or *MIR21* promotes anchorage-independent cell growth in mouse mammary epithelial cells. (a, b) Soft agar colony formation assays with *MMTV-ERBB2* mouse mammary epithelial cells transduced with control vector or lentiviral vector expressing the indicated genes. Representative images of soft agar formation colonies using 12-well plates are shown in (**a**) and relative expression levels of indicated genes and mature miR-21 are shown in (**b**). *** $p<0.001$; unpaired 2-tailed *t*-test. Data are presented as mean ± SD and are representative of 3 independent experiments.

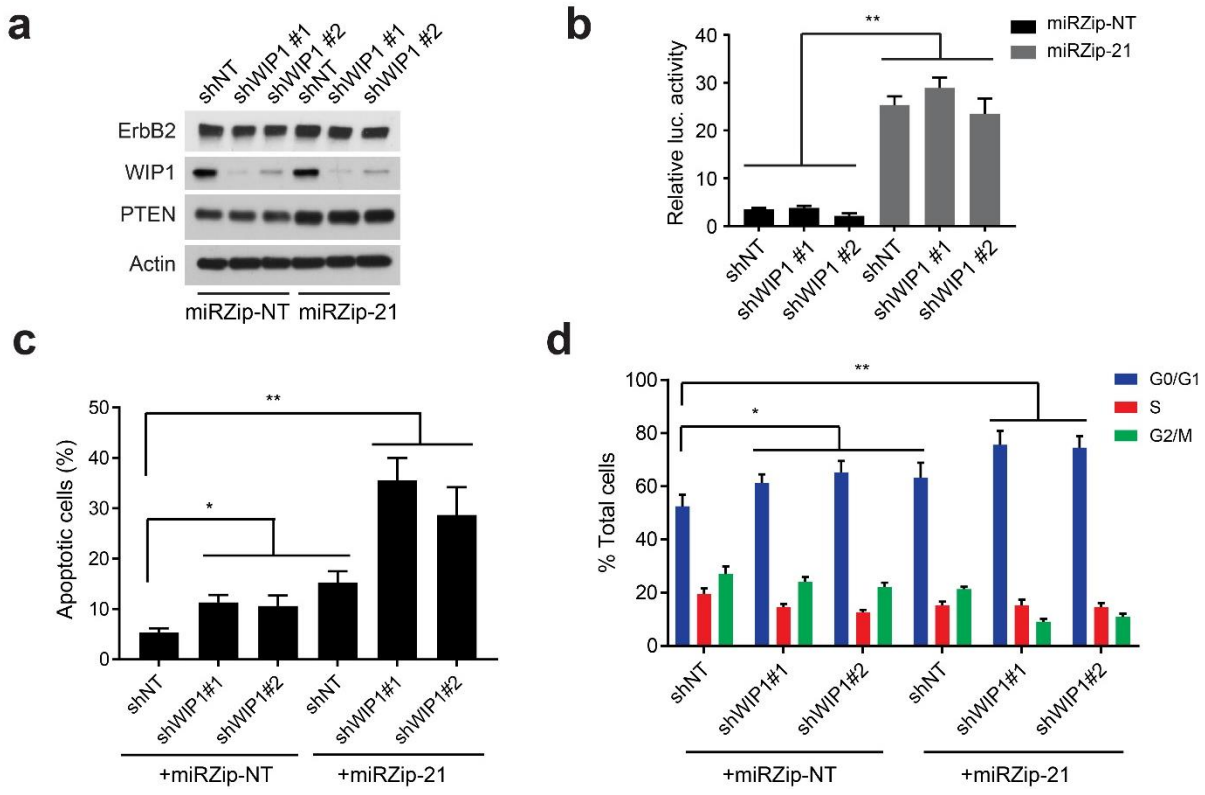

Supplementary Figure 3. Suppression of miR-21 and WIP1 inhibits proliferation and tumorigenic potential of mouse H605 cells. (**a, b**) Protein expression levels of ErbB2, WIP1 and PTEN in mouse H605 cells with stable knockdown of WIP1, miR-21 or both (**a**). Knockdown efficiency of miR-21 was measured by luciferase reporter assay (**b**). The luciferase activity of the reporter gene with miR-21-targeting 3'-UTR is negatively correlated with the level of miR-21. (**c, d**) The knockdown effect of WIP1, miR-21 or both on cell apoptosis (**c**) and cell cycle distribution (**d**). Cells were stained with Annexin V (**c**) or propidium iodide (**d**) and analyzed by flow cytometry 72 h post-induction of shWIP1 or anti-miRZip-21 expression. * p<0.05; ** p<0.01; *** p<0.001; unpaired 2-tailed t-test (**e, h**). Data are presented as mean ± SD and are representative of 3 independent experiments.

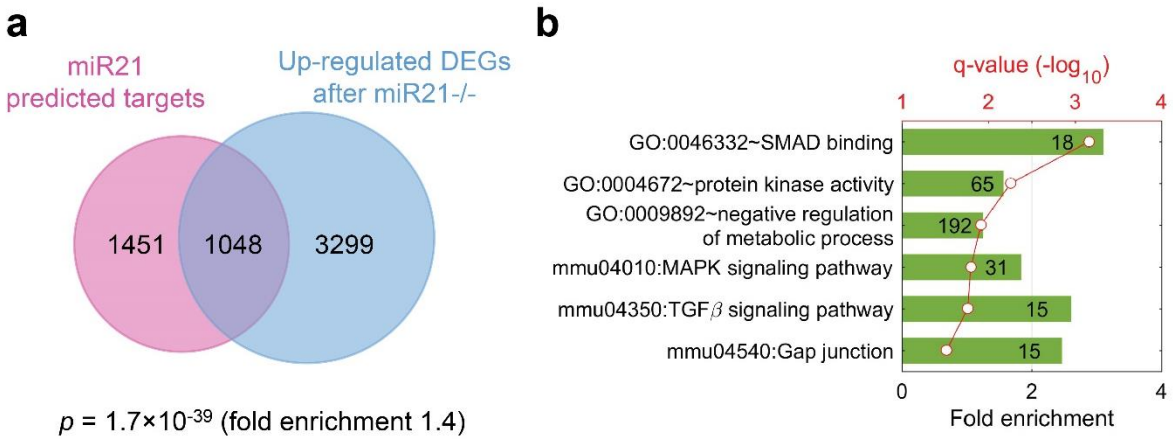

Supplementary Figure 4. miR-21 target gene expression and TGF-beta pathway mammary epithelial cells. (**a**) Venn diagram showing overlaps of upregulated genes in *MIR21-/-;MMTV-ErbB2* mammary epithelial cells with predicted miR-21 target genes. (**b**) Enrichment of TGF-β/Smad Signaling gene set in the mammary epithelial cells (MMECs) derived from *MIR21-/-;MMTV-ErbB2* mice (8-week old), as determined by gene ontology enrichment analysis.

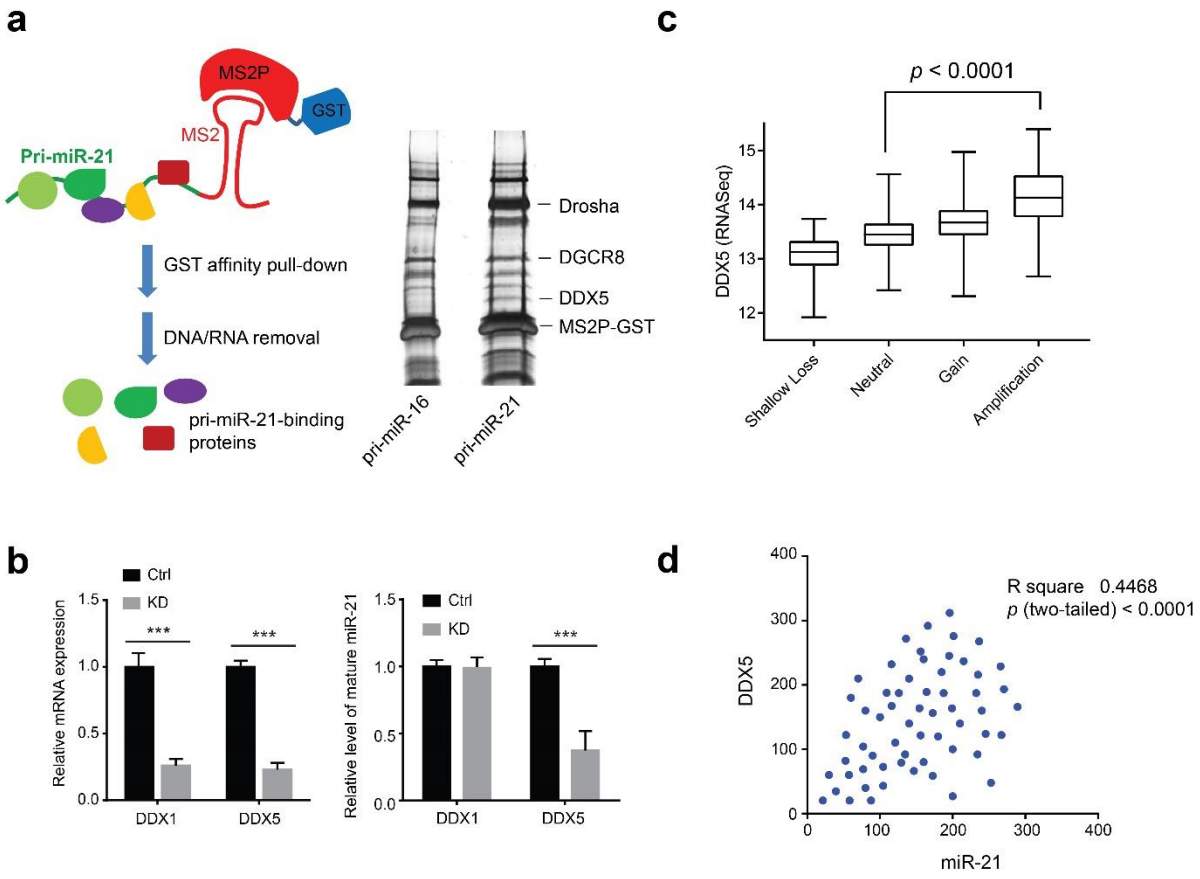

Supplementary Figure 5. *DDX5* gene is co-amplified with *MIR21* and its expression facilitates maturation of pri-miR-21. (a) DDX5 interacts with pri-miR-21 in the microprocessor. The assay is based on the addition of a specific bacteriophage MS2 RNA hairpin loop sequence to pri-miR-21, followed by co-expression of the MS2-tagged RNA together with GST-tagged MS2P that specifically binds MS2. The pri-miR-21 binding proteins were analyzed by gel electrophoresis and the protein bands of interest were determined by mass spectrometry. (**b**) The relative expression levels of mature miR-21 after depletion of DDX1 or DDX5 in MCF-7 cells as determined by qPCR. The efficiency of DDX1 and DDX5 knockdown was measured by qPCR as well (left panel). Student t-test, *** p<0.001. (**c**) A box-and-whisker plot was used to visualize DDX5 expresson levels in breast tumors. The Shapiro-Wilk test was applied to verify that mRNA expression does not follow a normal distribution in each group. (**d**) miR-21 levels are positively correlated with DDX5 expression levels in breast cancer. Intensity of miR-21 and DDX5 signals were scored in breast adenocarcinomas using tumor microarray and Pearson's correlation coefficient was analyzed by GraphPad Prism 6 software. Scoring = intensity (1, 2 or

3) x proportion (10-100%). *** $p<0.001$; unpaired 2-tailed *t*-test (**b, c**). Data are presented as mean ± SD and are representative of 3 independent experiments.

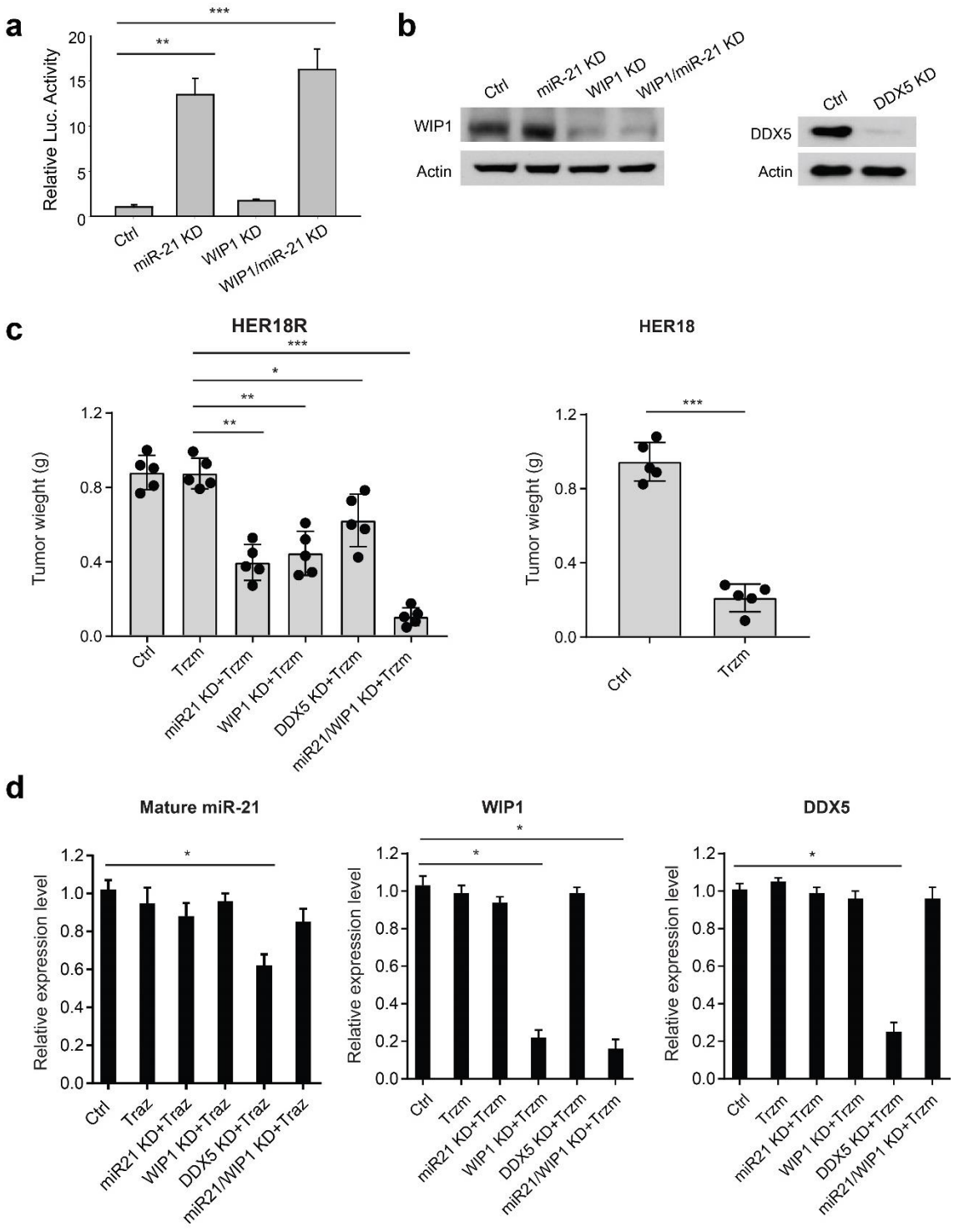

Supplementary Figure 6. Inhibition of miR-21 sensitizes HER2+ breast cancer cells to the treatment of trastuzumab. (**a**) Knockdown efficiency of miR-21 in Trastuzumab-resistant

HER18R cells was measured by luciferase reporter assay. The luciferase activity of the reporter gene with miR-21-targeting 3'-UTR is negatively correlated with the level of miR-21. (**b**) Western blot analyses were performed to show knockdown efficiency of WIP1 (left) or DDX5 (right) in the HER18R cells. (**c**) Tumor weight of xenograft tumors derived from orthotopicaly implanted isogenic parental or trastuzumab-resistant HER18 cells expressing Dox-inducible WIP1 or DDX5 shRNA or anti-miR21 oligonucleotides with trastuzumab treatment (5mg kg^{-1}, twice per week). (**d**) Quantification of knockdown efficiencies of miR-21, WIP1 or DDX5 in the xenografted tumor tissues described above. * $p<0.05$; ** $p<0.01$; *** $p<0.001$; unpaired 2-tailed *t*-test. Data are presented as mean ± SD and are representative of 3 independent experiments.

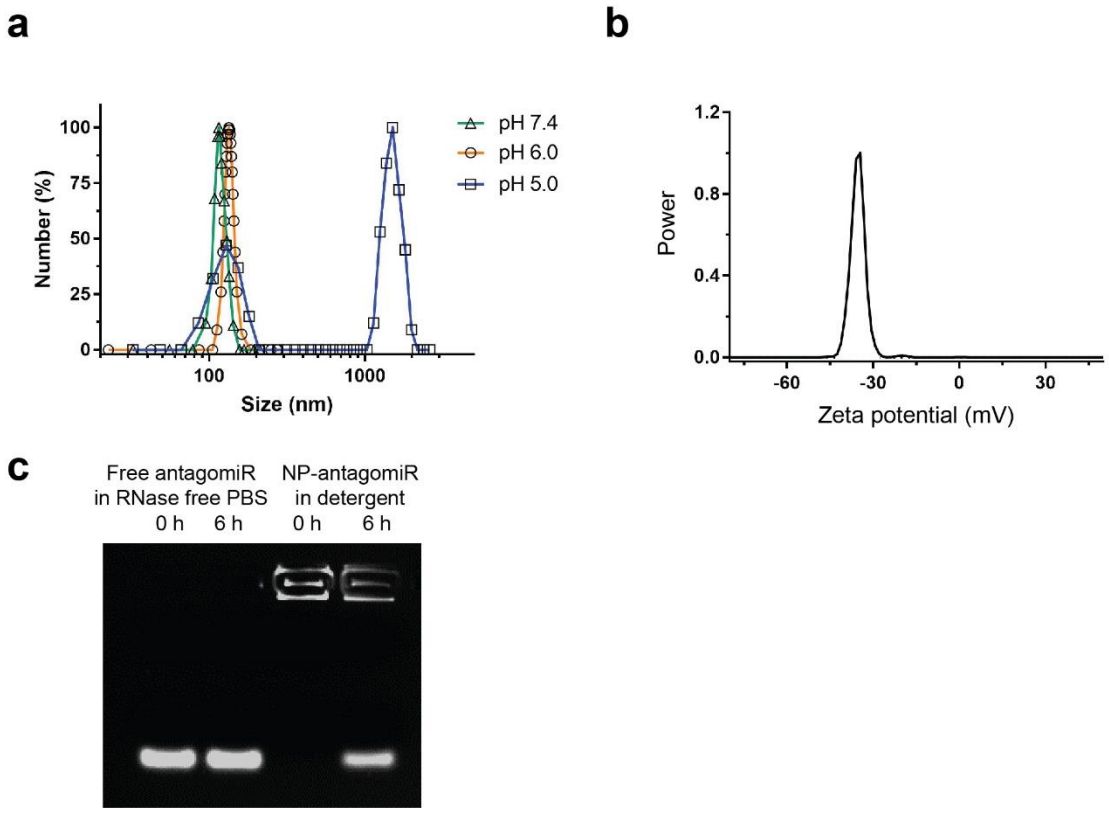

Supplementary Figure 7. Synthesis of nanoparticles for delivering WIP1 and miR-21 inhibitors. (**a**) Nanoparticle size distribution determined by dynamic light scattering (DLS) in pH 7.4 (polydispersity index (PDI), 0.05), pH 6.0 (PDI, 0.08), and pH 5.0 (PDI, 0.285), respectively. (**b**) Surface zeta potential of in-MW@NP nanoparticles. (**c**) Electrophoretic assay of free anti-miR21 inhibitor and in-MW@NP at different incubation time points in RNase-free buffer or detergent solution at 37 ºC. Data are representative of 3 independent experiments.

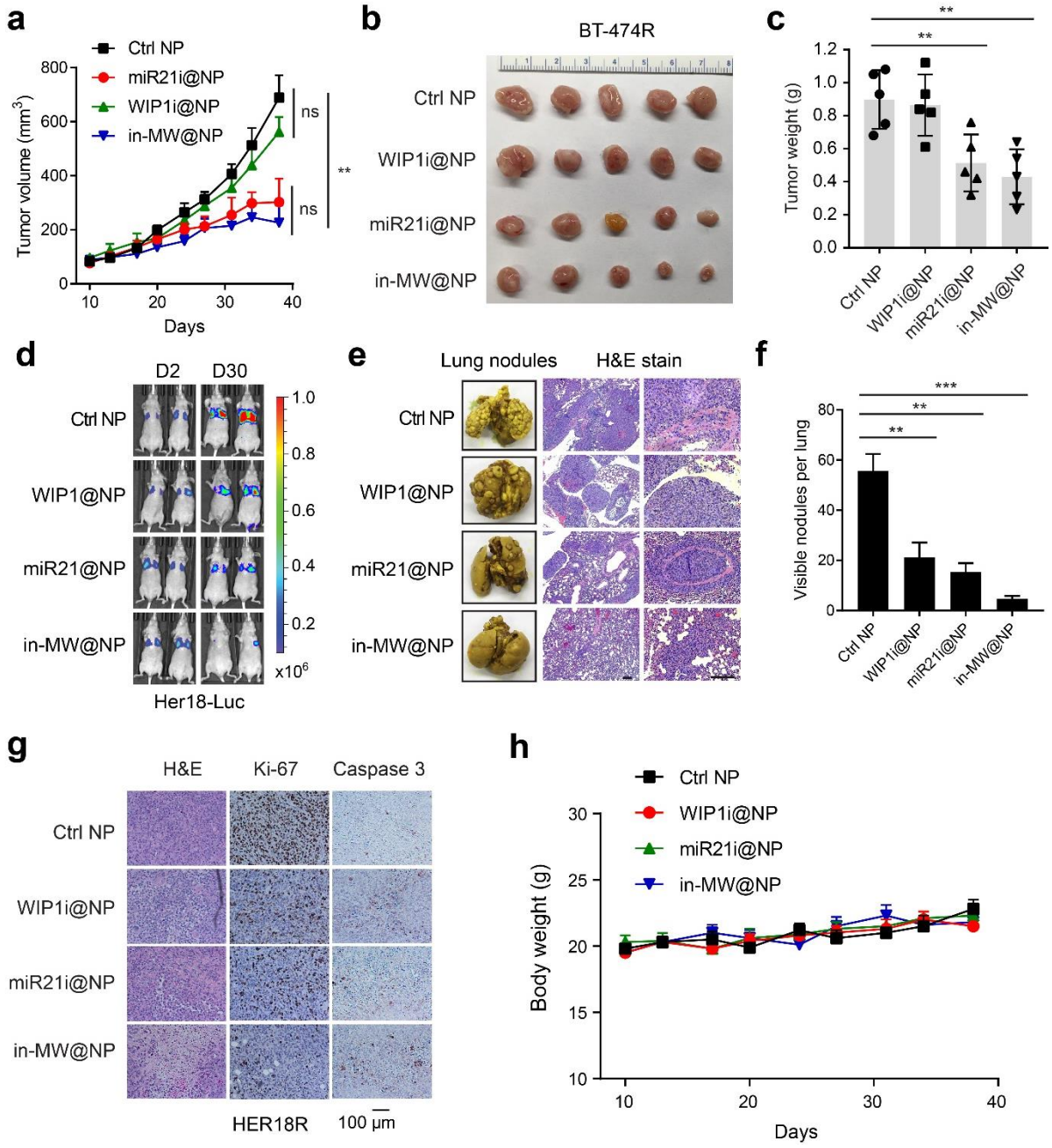

Supplementary Figure 8. In vivo efficacy of nanoparticle-encapsulated WIP1 and miR-21 inhibitors in trastuzumab-resistant breast tumor models. (**a-c**) Tumor growth curves (**a**), gross tumor images (**b**) and tumor weight (**c**) of xenograft tumors derived from orthotopically implanted trastuzumab-resistant BT474R cells. Once tumors were palpable, mice were randomly divided to 4 groups and then treated with either control, WIP1 and/or miR-21 inhibitor nanoparticles (twice per week) intravenously. (**d-f**) Graphic representation of bioluminescent images (**d**), lung lesions (**e**) and number of metastatic nodules from mice injected with 5×10^6

HER18R cells through tail vein into female NU/J mice. On day 3, mice were randomly divided to 4 groups and then treated with either control, WIP1 and/or miR-21 inhibitor nanoparticles (twice per week) intravenously. Scale bar: 100 μm. (**g**) Representative images of H&E, Ki-67 (cell proliferation) and cleaved caspase-3 (apoptosis) staining in orthotopically implanted HER18R tumor tissues. Scale bar: 100 μm. (**h**) Changes in the body weights of NU/J mice with treatments as described in the HER18R groups. ** $p<0.01$; *** $p<0.001$; unpaired 2-tailed *t*-test. Data are presented as mean ± SD.

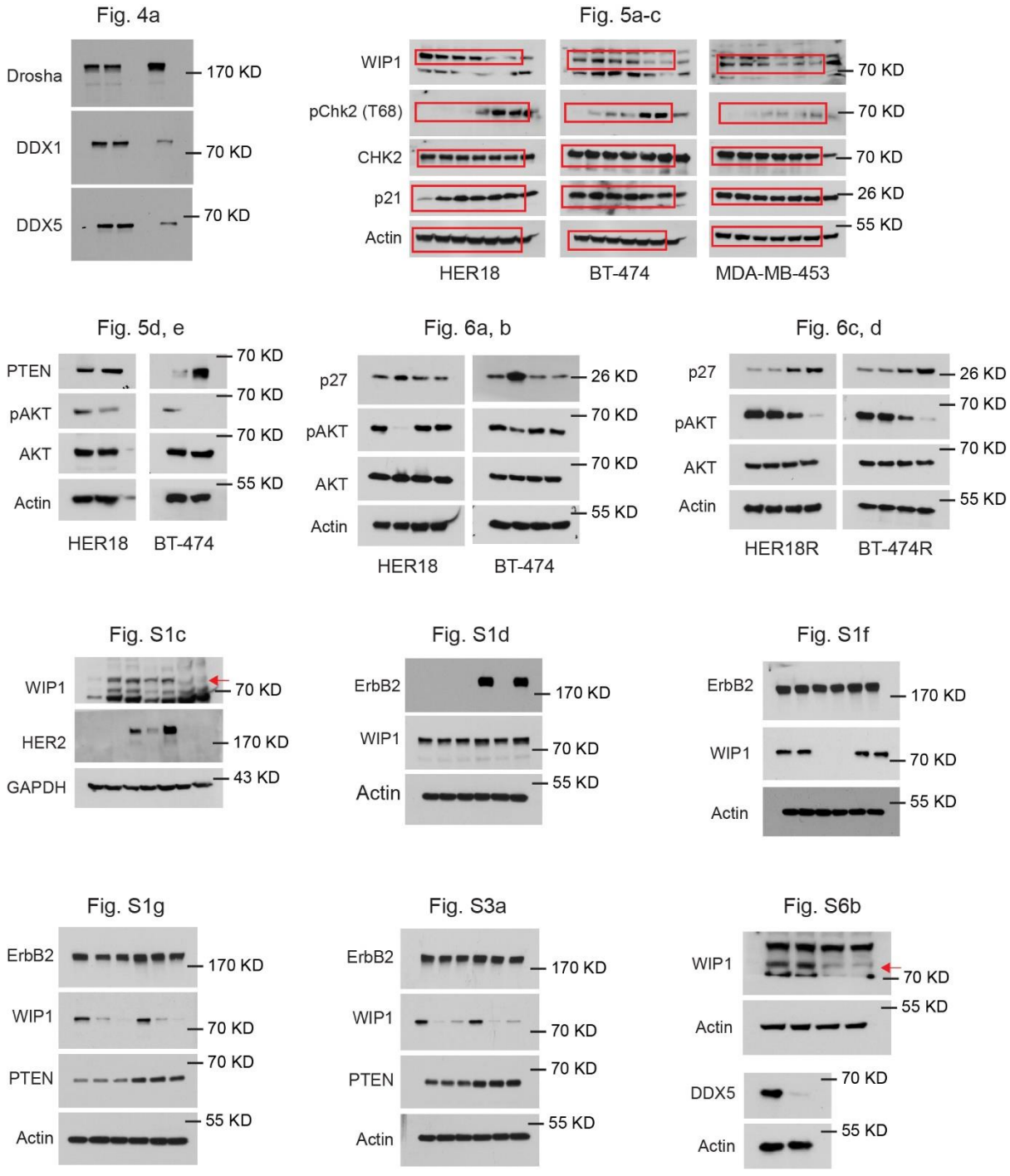

Supplementary Figure 9. Uncropped western blots.

Supplementary Table 1. Primer sequences for real-time PCR.

Name	Sequence	Species
pri-miR-21-F	ttttgttttgcttgggagga	Human
pri-miR-21-R	agcagacagtcaggcaggat	Human
pri-miR-16-F	gctcttatgatagcaatgtcagca	Human
pri-miR-16-R	caaccttacttcagcagcacag	Human
pri-miR-200a-F	gatgcaagggtcagaagggc	Human
pri-miR-200a-R	gagccatctggcccggacg	Human
DDX1-F	ttgatgggaaagttacctacgg	Human
DDX1-R	caagatgcaggaaagatgtctg	Human
DDX5-F	atgtcgggttattcgagtgacc	Human
DDX5-R	tgtgcgcctagccaaatcag	Human
WIP1-F	ctgtactcgctgggagtgag	Human
WIP1-R	gttcgggctccacaacgatt	Human
pri-miR-21-F	gactgttgaatctcatggcaac	Mouse
pri-miR-21-R	tgctgggtaatgtttgaatgaa	Mouse
pri-miR-16-F	gctcctatgatagcaatgtcagc	Mouse
pri-miR-16-R	caaccttacttcagcagcacag	Mouse
DDX1-F	aatgaaatgcagctactttccg	Mouse
DDX1-R	ctgtctacatgacgtcagaagg	Mouse
DDX5-F	cgggatcgagggtttggtg	Mouse
DDX5-R	gcagctcatcaagattccacttc	Mouse
WIP1-F	gatgtatgtagcgcatgtaggtg	Mouse
WIP1-R	gttctggcttgtgatcttgtgt	Mouse
BMPR2-F	ttgggataggtgagagtcgaat	Mouse
BMPR2-R	tgtttcacaagattgatgtcccc	Mouse
MAP2K3-F	gcctcagaccaaaggaaaatcc	Mouse
MAP2K3-R	ggtgtggggttggacacag	Mouse
PIK3R1-F	acaccacggtttggactatgg	Mouse
PIK3R1-R	ggctacagtagtgggcttgg	Mouse
PTEN-F	tggattcgacttagacttgacct	Mouse
PTEN-R	gcggtgtcataatgtctctcag	Mouse
SKI-F	caaaacagacgacacttcctca	Mouse
SKI-R	cagccgaggctcttattggag	Mouse
SMAD7-F	ggccggatctcaggcattc	Mouse
SMAD7-R	ttgggtatctggagtaaggagg	Mouse
SOS2-F	caagatgttgaggaacgagttca	Mouse
SOS2-R	tgtccacaggtagtaagagagga	Mouse
TLR4-F	atggcatggcttacaccacc	Mouse
TLR4-R	gaggccaattttgtctccaca	Mouse
BMPR1B-F	ccctcggcccaagatccta	Mouse
BMPR1B-R	caacaggcattccagagtcatc	Mouse

INHBA-F	tgagaggatttctgttggcaag	Mouse
INHBA-R	tgacatcgggtctcttcttca	Mouse
MAP2K4-F	aatcgacagcacggtttactc	Mouse
MAP2K4-R	tgaaatcccagtgttgttcagg	Mouse
MAPK1-F	ggttgttcccaaatgctgact	Mouse
MAPK1-R	caacttcaatcctcttgtgaggg	Mouse
NRAS-F	actgagtacaaactggtggtgg	Mouse
NRAS-R	tcggtaagaatcctctatggtgg	Mouse
SMAD2-F	atgtcgtccatcttgccattc	Mouse
SMAD2-R	aaccgtcctgttttctttagctt	Mouse
SMURF2-F	aaacagttgcttgggaagtca	Mouse
SMURF2-R	tgctcaacacagaaggtatggt	Mouse
SOS1-F	caagttcaccctactcttgagtc	Mouse
SOS1-R	catcagctattgcccacttatca	Mouse
CASP3-F	atggagaacaacaaaacctcagt	Mouse
CASP3-R	ttgctcccatgtatggtctttac	Mouse
SYNJ1-F	ggaagaatgtctcatgttcgagt	Mouse
SYNJ1-R	ccagatagtgcagcatggtatca	Mouse
PPP2R1B-F	tcgcggttttaatcgacgag	Mouse
PPP2R1B-R	ctaccccgagtgctagagcta	Mouse